MJoSHT
Malaysian Journal of Science, Health & Technology
[mjosht.usim.edu.my]

*Article*

# Simulation of a Photoacoustic-Based Gold Authentication System for Tungsten Inclusion Detection Using COMSOL Multiphysics

Nur Izzatul Syahzanani Abd Ghani, Juliza Jamaludin, Marinah Othman, Irneza Ismail, Fatinah Mohd Rahalim, Mahfuzah Samirah Ideris, and Firdaus Zaid

Faculty of Engineering and Built Environment, Universiti Sains Islam Malaysia, Bandar Baru Nilai, Nilai, 71800, Malaysia.

*Correspondence should be addressed to:*
*Juliza Jamaludin; juliza@usim.edu.my*

*Article Info*
*Article history:*
*Received:20 August 2025*
*Accepted: 16Mac 2026*
*Published: 15 April 2026*
*Academic Editor:*
*Wan Maisarah Wan Mukhtar*
*Malaysian Journal of Science, Health & Technology*
*MJoSHT2025, Volume 12, Issue No. 1*
*eISSN: 2601-0003*
*https://doi.org/10.33102/mjosht.506*


***Abstract*— The increasing presence of counterfeit gold, especially with tungsten inclusions, poses a significant challenge to the authenticity of gold trading. This research presents a photoacoustic sensing (PAS) method for detecting tungsten inclusions in gold bars. Photoacoustic sensing leverages laser-induced acoustic waves to identify material discrepancies based on their thermal and optical characteristics. This approach enhances the detection capabilities by focusing on the photoacoustic response generated by the interaction of the gold and tungsten matrix with laser light, making it a more reliable and efficient non-destructive testing method. The proposed method is modelled and simulated using COMSOL Multiphysics, providing a simulation-based solution for gold verification. This research aims to contribute to the promotion of fair-trade practices by ensuring the authenticity of gold, aligning with the Sustainable Development Goals (SDGs), specifically SDG 8: Decent Work and Economic Growth, and SDG 12: Responsible Consumption and Production.**

***Keywords*— Gold authentication; photoacoustic sensing; tungsten inclusion; non-destructive testing**

## I. INTRODUCTION

The increasing presence of counterfeit gold, particularly in the form of tungsten-infiltrated gold bars, represents a significant challenge to the authenticity of gold trading [1]. High-profile cases highlight the growing sophistication of such fraud. In 2012, tungsten-filled gold bars were discovered in Manhattan when a dealer drilled into a 10-ounce bar and found a tungsten core beneath a thin gold shell [2]. Similarly, in 2017, a gold bar bearing certification from an official mint was discovered to contain tungsten, raising concerns about the reliability of even formally certified bullion [3]. In 2020, a major gold fraud scandal revealed that counterfeit gold bars made of gold-plated copper had been used as collateral to secure loans amounting to approximately $2.8 billion [4]. These incidents underline the vulnerabilities of current gold authentication methods.

The conventional methods used to verify gold authenticity, such as density measurements, X-ray fluorescence (XRF), and ultrasonic testing (UT), are often inadequate when faced with more advance counterfeiting techniques, such as tungsten-filled gold. Tungsten's similar density to gold makes it particularly difficult to detect using conventional methods, which typically rely on differences in material densities [5].

Moreover, in Malaysia, the Pawnbroker Act 1972 mandates that pawned items must be preserved in their original condition until the transaction is completed [6]. This legal requirement prohibits the use of destructive testing methods, further limiting options for authenticating gold.

This research introduces a photoacoustic sensing (PAS) technique to address these limitations. PAS leverages the interaction between light and matter to produce ultrasonic waves, which can be detected to assess material properties [7]. By using a pulsed laser to induce localized heating within the material, PAS generates acoustic waves that provide valuable insights into the material's internal structure . This method capitalizes on the differences in optical absorption and thermal expansion between gold and tungsten, making it a promising approach for detecting tungsten inclusions even when they are deeply embedded within the gold matrix [8].

The primary aim of this study is to develop a simulation-based methodology using COMSOL Multiphysics to analyze the behavior of photoacoustic waves as its interact with gold and tungsten. By simulating these interactions, this research seeks to enhance the reliability and sensitivity of gold authentication systems, providing a non-destructive, accurate, and efficient solution to detect counterfeit gold. The results of this study could help improve non-destructive testing (NDT) methods used in the gold industry and promote fair trade practices by ensuring the authenticity of gold in the market.

In addition, this research aligns with the Sustainable Development Goals (SDGs), particularly SDG 8: Decent Work and Economic Growth, and SDG 12: Responsible Consumption and Production. By ensuring the integrity of gold trade, the study contributes to the fight against fraud and promotes ethical business practices within the precious metals industry.

## II. METHODS

This study utilizes COMSOL Multiphysics to simulate the photoacoustic interaction between gold and tungsten materials under laser irradiation. The primary objective is to investigate the photoacoustic effects and the stress distributions in both materials at different laser wavelengths.

### *A. Model Description*

Initially, a 1mm³ cube model was created to represent the materials under study referring to Figure 1. The choice of this model size was made to balance between achieving sufficient resolution for material interaction analysis and minimizing computational time. A larger model would require significantly more computational resources, potentially extending the simulation time excessively. The cube geometry was chosen for simplicity and computational efficiency.

To evaluate the system's ability to detect tungsten inclusions, composite models were developed with spherical tungsten inclusions embedded within a gold matrix. The model setup remained similar to the pure material simulations, except for the inclusion geometry.

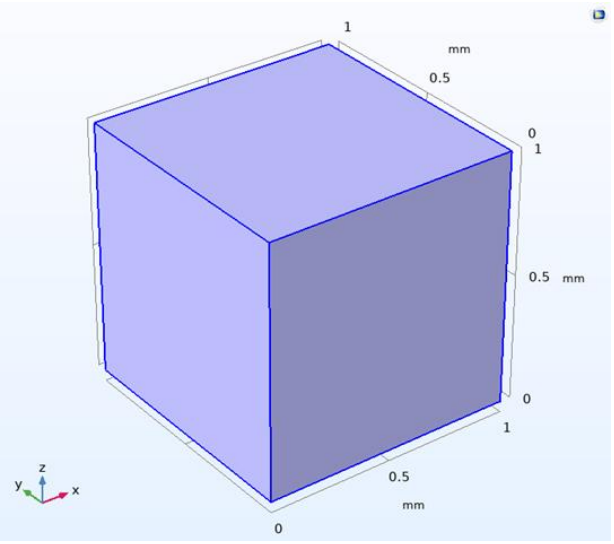

Figure 1. Geometry model shape

For the first configuration, a single spherical tungsten inclusion with a diameter of 0.2 mm was randomly positioned inside the 1 mm³ gold cube, as shown in Figure 2. This configuration represents a minimal adulteration scenario where a discrete tungsten core is concealed within the gold matrix.

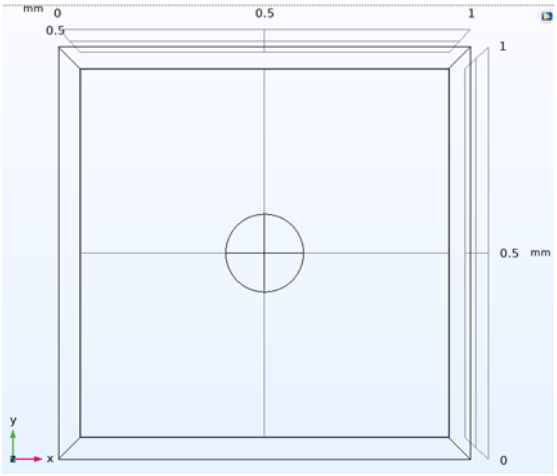

Figure 2. Geometry model for a single tungsten inclusion

The second configuration featured multiple spherical tungsten inclusions of varying sizes (0.1 mm to 0.3 mm in diameter) distributed randomly throughout the gold matrix, as shown in Figure 3. This case simulates more complex adulteration patterns where tungsten particles are dispersed within the gold structure, creating a more challenging detection scenario. Both configurations maintained identical material properties, laser excitation parameters, and boundary conditions as the pure material simulations for consistent comparison.

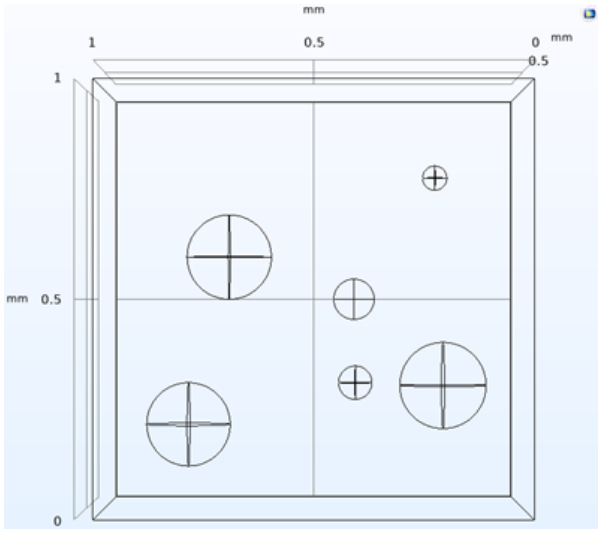

Figure 3. Geometry model for multiple tungsten inclusions

## B. Simulation Parameters

The parameters for the model were defined using COMSOL's Model Builder, with material properties for gold and tungsten specified based on standard values. These included properties such as thermal conductivity, density, specific heat capacity, and absorption coefficients relevant to each material's behaviour under laser irradiation. The simulation was run for three different laser wavelengths [9]:

- 850nm
- 960nm
- 1310nm

These wavelengths were selected as they are commonly used in photoacoustic imaging and represent typical near-infrared (NIR) laser sources. Each wavelength was tested to examine its effect on the stress distribution (Von Mises stress) within both gold and tungsten [10]. The study was limited to three discrete wavelengths (850 nm, 960 nm, and 1310 nm) representative of the near-infrared spectrum. Other wavelengths outside this range were not examined as they fall outside the scope of this initial simulation study.

The parameter values are stated as below Table 1. The absorption coefficient (mu_a) value is wavelength-dependent and varies based on both the material and the wavelength being measured. If other wavelengths are used, this value will need to be adjusted according to the specific absorption properties of the material at those wavelengths. Table 2 is the corresponding value of absorption coefficient based on each wavelength of the material [11].

TABLE 1. PARAMETER SETTINGS

| Name | Value | Description |
|---|---|---|
| **I0** | 1E8 [W/m²] | Peak laser intensity |
| **mu_a** | Refer Table 2 | Vary depending on wavelength value |
| **x0** | 5E-4 [m] | Laser beam center coordinates |
| **y0** | 5E-4 [m] | Laser beam center coordinates |
| **w** | 1E-4 [m] | Beam radius |
| **t_p** | 5E-9 [s] | Time at peak of pulse |
| **tau** | 2E-9 [s] | Laser pulse half-duration |

TABLE 2. ABSORPTION COEFFICIENT VALUE

| Material | Wavelength Value (nm) | Absorption Coefficient Value [1/mm] |
|---|---|---|
| Gold | 850 | 7.4540e4 |
| | 960 | 7.8370e4 |
| | 1310 | 8.3721e4 |
| Tungsten | 850 | 4.8517e5 |
| | 960 | 5.1007e5 |
| | 1310 | 5.4709e5 |

## C. Physics Modules

The following physics modules were applied to simulate the photoacoustic effect:

*1) Heat Transfer in Solids (HT):* This module was used to simulate the heat generation and thermal diffusion within the gold and tungsten materials when irradiated by a pulsed laser. The laser absorption at each wavelength leads to localized heating, which causes thermal expansion and subsequently initiates photoacoustic wave generation.

*2) Solid Mechanics (Solid):* The module was used to analyze the stress distribution within the materials as a result of the thermal expansion. The Von Mises stress was observed at various stages of the simulation to evaluate the material deformation caused by the photoacoustic effect.

# III. RESULTS

The simulation results are visualized on the top surface of the cube model. The square surface represents the area where the laser is applied, and the photoacoustic response is measured. The square surface plot is a direct result of visualizing data on one face of the cube. The simulation results for gold and tungsten materials at 850 nm, 960 nm, and 1310 nm reveal that there is minimal variation in the Von Mises stress distribution across these wavelengths for both materials. The stress distributions at each wavelength are similar, with no significant differences observed in the overall stress variation.

Since the earlier simulations on pure gold and pure tungsten demonstrated that all three wavelengths (850 nm, 960 nm, and 1310 nm) produced similar stress distributions, the composite model simulations were conducted using only a single wavelength. The 850 nm wavelength was selected for simulations conducted at the inclusion composite models as it is the most cost-effective, widely available, and commonly used in photoacoustic applications. This approach reduces computational time while maintaining reliable results, as the absorption coefficients across the tested near-infrared range are relatively similar in magnitude, resulting in comparable stress responses regardless of wavelength variation within this spectrum.

## A. Gold Material

At 850 nm in Figure 4, the stress distribution in gold is relatively uniform and shows a tight clustering of stress values. This indicates that gold absorbs the laser energy in a consistent manner, resulting in moderate thermal expansion and a

relatively gentle photoacoustic effect. The stress variation is small, suggesting that the response of gold to this wavelength is not as pronounced compared to other materials.

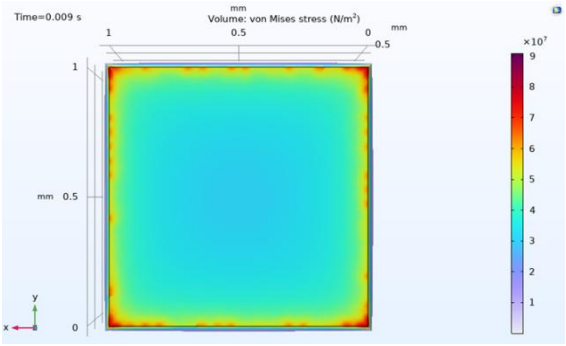


Figure 4. Gold Stress distribution at 850 nm

At 960 nm in Figure 5, the stress distribution shows little to no change compared to the 850 nm wavelength, remaining tightly clustered. This suggests that while gold absorbs slightly more energy at 960 nm, the stress variation does not significantly increase. The photoacoustic effect at this wavelength is still relatively moderate, like the response at 850nm.

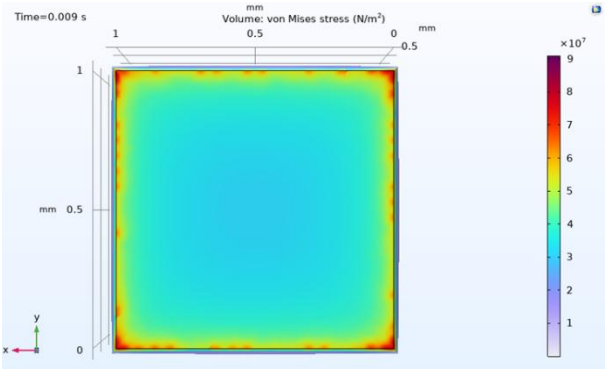


Figure 5. Gold Stress distribution at 960 nm

At 1310 nm in Figure 6, the stress distribution in gold is still quite similar to the previous wavelengths, with only slight increases in stress at certain regions. The photoacoustic response at 1310 nm is slightly more pronounced than at 850 nm and 960 nm, but the difference is not significant. This shows that while gold absorbs more energy at this wavelength, the resulting thermal expansion and stress are still within a narrow range.

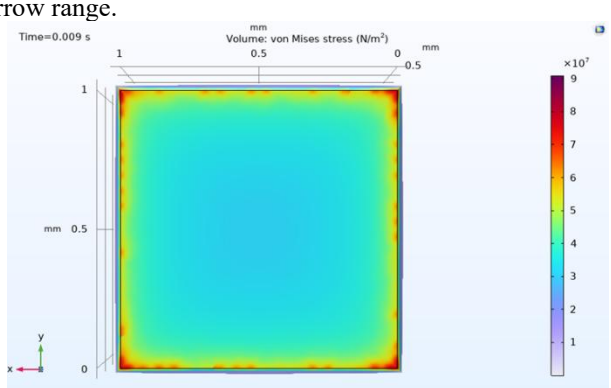


Figure 6. Gold Stress distribution at 1310 nm

*B. Tungsten Material*

For tungsten at 850 nm in Figure 7, the stress distribution is noticeably wider compared to gold, indicating greater variability in the material's response. The stress values are more spread out, suggesting that tungsten absorbs laser energy differently, resulting in higher thermal expansion and a more pronounced photoacoustic effect.

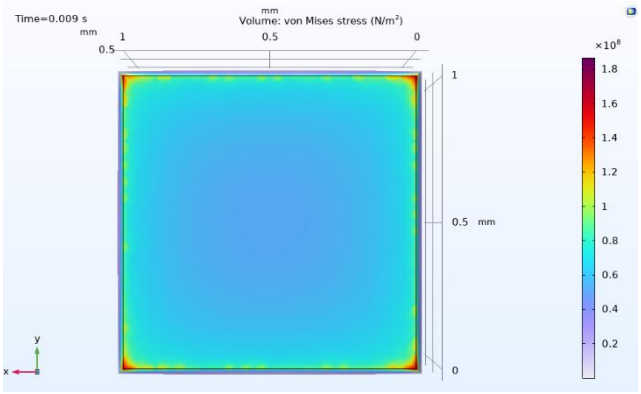


Figure 7. Tungsten Stress distribution at 850 nm

At 960 nm in Figure 8, the stress distribution in tungsten does not show a significant change compared to 850 nm. The spread of stress values is still relatively wide, but the overall distribution does not differ greatly from the previous wavelength. The photoacoustic response at 960 nm appears to be similar to that at 850 nm, despite the increased absorption at this wavelength.

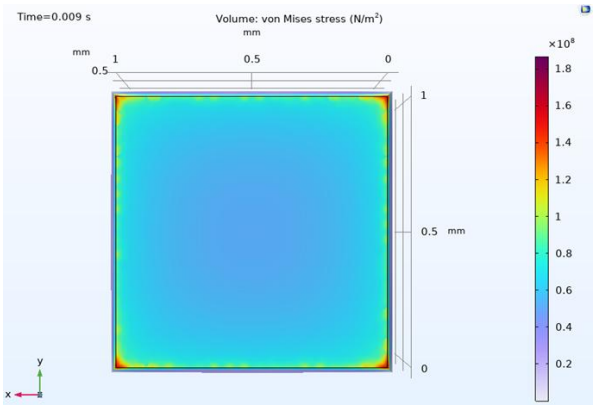


Figure 8. Tungsten Stress distribution at 960 nm

At 1310 nm in Figure 9, the stress distribution in tungsten remains similar to the previous wavelengths. Although tungsten absorbs slightly less energy at 1310 nm, the stress variation is still comparable to 850 nm and 960 nm, showing no dramatic change in the overall response. The photoacoustic effect is noticeable, but again, the variation in stress is not significantly different from the other wavelengths.

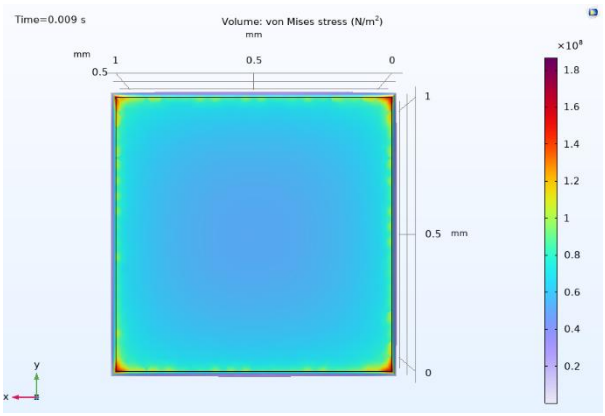


Figure 9. Tungsten Stress distribution at 1310 nm

A comparative evaluation of von Mises stress distributions between two simulations shows a significant discrepancy in stress magnitudes. On the pure gold model, the stress peaks are at approximately $10^7$ N/m² (10 MPa). In contrast, the pure tungsten model reaches its peak around $10^8$ N/m² (100 MPa). This order-of-magnitude variation can be attributed to differences in both materials properties and laser- induced thermal responses.

### *C. Gold-Tungsten Composite with Single Inclusion*

Figure 10 shows the stress distribution for the gold matrix with a single tungsten inclusion. Based on the results, the von Mises stress distribution does not highlight significant stress on the tungsten inclusion itself. Instead, the highest stress concentrations are observed along the edges of the gold matrix, particularly at the boundary between the tungsten and the surrounding material. The peak stress value at the boundary is approximately $8 \times 10^7$ N/m², as indicated by the colour scale. The interface between the tungsten inclusion and the gold matrix experiences localized stress, as shown by the red regions in the plot, while the stress within the tungsten itself remains relatively low.

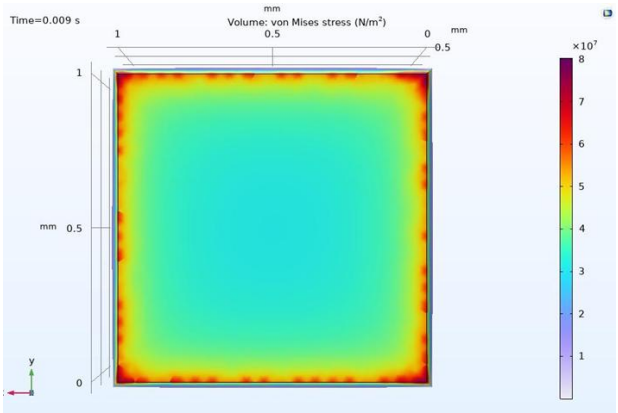


Figure 10. Stress distribution for single tungsten inclusion

### *D. Gold-Tungsten Composite with Multiple Inclusions*

Figure 11 presents the stress distribution for the gold matrix with multiple tungsten inclusions of varying sizes and locations. The simulation shows distinct stress concentration at the interfaces between the tungsten inclusions and the surrounding gold. In this configuration, only the tungsten inclusions closer to the surface of the gold matrix are visible in terms of their impact on the von Mises stress distribution. The proximity of certain inclusions near the surface produces a yellowish region indicating peak stress values around those areas. Inclusions located deeper within the gold matrix do not show significant stress concentration on the surface, as the stress effects become more diffused with increasing distance from the surface. This highlights the influence of inclusion depth on surface stress visibility, with deeper inclusions having a lesser visible impact on the surface stress field.

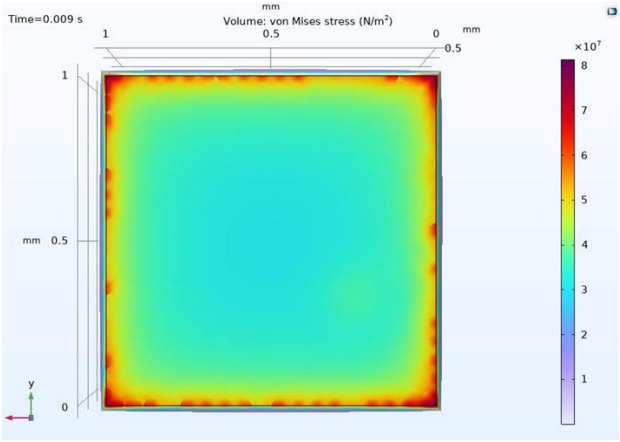


Figure 11. Stress distribution for multiple tungsten inclusions

### *E. Comparison between material*

TABLE 3. STRESS DISTRIBUTION ON EACH WAVELENGTH

| | Gold | Tungsten |
|---|---|---|
| 850 nm | 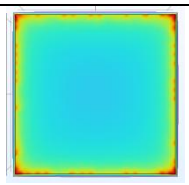 |  |
| 960 nm | 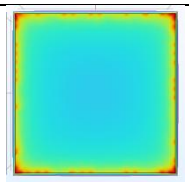 |  |
| 1310 nm | 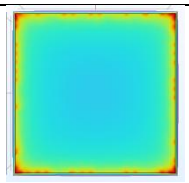 |  |

### *F. Comparison between composites*

TABLE 4. STRESS DISTRIBUTION BETWEEN THE CASES

| | Single Inclusion | Multiple Inclusion |
|---|---|---|
| 850 nm | 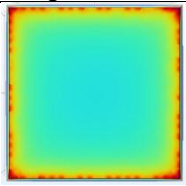 | 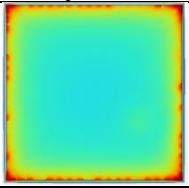 |

## IV. DISCUSSION

The dot plot and ANOVA test results provide valuable insights into the differences in stress response (Von Mises stress) between gold and tungsten materials, the effects of different laser wavelengths (850 nm, 960 nm, 1310 nm) on these materials, as well as the composite of single tungsten inclusion and multiple tungsten inclusion.

### *A. Dot Plot Analysis*

Figure 12, 13 and 14 below are the dot plot comparison made between material and wavelength. The dot plot for gold (Figure 12) shows a more concentrated range of stress values, indicating less variation in the response compared to tungsten. Gold's response is more consistent across the measured wavelengths, suggesting that it has a more uniform material property when subjected to the laser-induced stress.

For Figure 13, tungsten, on the other hand, exhibits a broader spread of stress values, particularly at the higher wavelengths (960 nm and 1310 nm), indicating a higher variability in its stress response. This could be attributed to tungsten's higher absorption coefficient at these wavelengths, leading to more significant thermal expansion and greater stress formation.

For the observation made on the analysis comparison by wavelengths, the three of the wavelengths produces similar output. This is because of the absorption coefficients value between the two materials across the three wavelengths are similar to each other, hence producing the same frequency stress distribution.

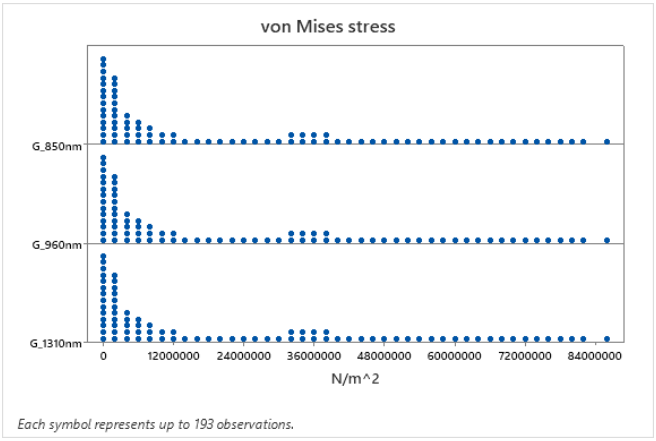


Figure 12. Comparison of gold stress distribution between wavelengths

Figure 15 presents the dot plot comparison between single and multiple tungsten inclusions in the gold matrix. For the single inclusion case, the dot plot reveals a concentration of von Mises stress values around the lower stress range, with a sharp peak at 0 to 2,400,000 N/m². The distribution is relatively narrow, with a visible gap between the final data points at the far-right end of the plot, suggesting that the stress diminishes before reaching the model boundary, reflecting a more confined stress propagation pattern.

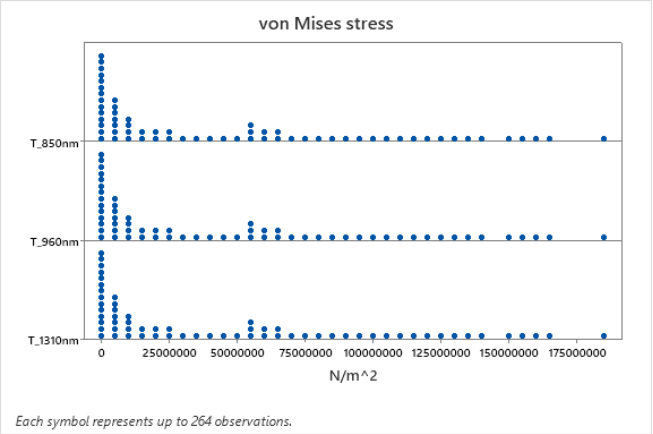


Figure 13. Comparison of tungsten stress distribution between wavelengths

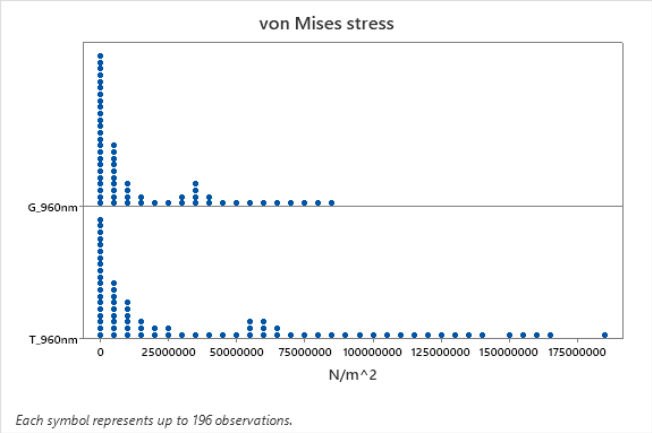


Figure 14. Comparison of stress distribution between material at 960 nm

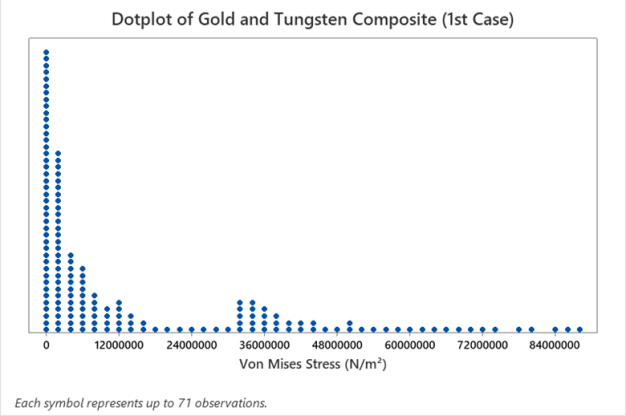


Figure 15. Stress distribution reading for a single tungsten inclusion

For the multiple inclusions case in Figure 16, the dot plot shows a broader distribution of stress values. While the stress peak at the lower range is similar to the single inclusion case, the distribution is spread out over a wider range with more data points extending beyond the 2,400,000 N/m² mark. At the far-right end of the plot, the data points remain continuous with no visible gap, suggesting that the stress field extends more uniformly towards the model boundary. This difference highlights how the number and positioning of inclusions influence not only the magnitude of stress but also the extent of its propagation within the material.

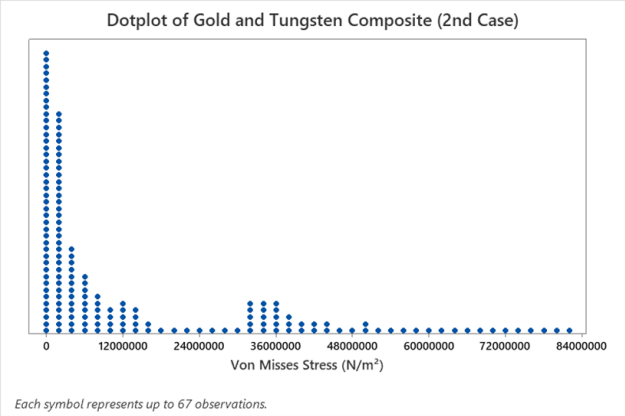


Figure 16. Stress distribution reading for multiple tungsten inclusions.

## B. ANOVA Test

The ANOVA test was used to assess whether there is a statistical difference in the stress responses between the materials (gold vs. tungsten) and the wavelengths (850 nm, 960 nm, 1310 nm), and the composites.

### 1. Null Hypothesis for Material Comparison

The null hypothesis for the material comparison states that there is no significant difference in the stress response between gold and tungsten. The alternative hypothesis suggests that there is a significant difference in the stress response between the two materials. The p-value obtained from the ANOVA test will determine whether to accept or reject the null hypothesis. If the p-value is greater than 0.05, the null hypothesis is accepted, indicating no significant difference in the stress response between the two materials. Conversely, if the p-value is less than 0.05, the null hypothesis is rejected, suggesting a significant difference in stress between gold and tungsten.

### 2. Null Hypothesis for Wavelength Comparison

The null hypothesis for wavelength comparison states that there is no significant difference in the stress response across the three wavelengths (850 nm, 960 nm, 1310 nm). The alternative hypothesis for wavelength comparison states that there is a significant difference in stress response across the wavelengths. Similarly, the p-value from the ANOVA test for wavelength comparison will determine whether the stress response significantly differs across the wavelengths. A p-value greater than 0.05 would suggest that there is no significant difference in stress response across the wavelengths, while a p-value less than 0.05 would indicate that the stress response is significantly affected by the wavelength.

### 3. Null Hypothesis for Inclusion Comparison

The null hypothesis states that there is no significant difference in the stress response between single and multiple tungsten inclusions in the gold matrix. The alternative hypothesis suggests that there is a significant difference in the stress response between the two configurations. The p-value obtained from the ANOVA test will determine whether to accept or reject the null hypothesis. If the p-value is greater than 0.05, the null hypothesis is accepted, indicating no significant difference in the stress response between the two configurations. Conversely, if the p-value is less than 0.05, the null hypothesis is rejected, suggesting a significant difference in stress between single and multiple inclusions.

Intra-Material Analysis (Gold Material):

- Null Hypothesis ($H_0$)

*There is no statistically significant difference in mean Von Mises stress among gold samples irradiated at 850 nm, 960 nm, and 1310 nm wavelengths.*

- Alternative Hypothesis ($H_1$)

*At least one wavelength produces a statistically significant difference in mean stress for gold.*

Intra-Material Analysis (Tungsten Material):

- Null Hypothesis ($H_0$)

*There is no statistically significant difference in mean Von Mises stress among tungsten samples irradiated at 850 nm, 960 nm, and 1310 nm wavelengths.*

- Alternative Hypothesis ($H_1$)

*At least one wavelength produces a statistically significant difference in mean stress for tungsten.*

Intra-Material Analysis (Gold-Tungsten Composite):

- Null Hypothesis ($H_0$)

*There is no statistically significant difference in mean Von Mises stress between gold-tungsten composites with single inclusion and gold-tungsten composites with multiple inclusions when irradiated at 850 nm wavelength.*

- Alternative Hypothesis ($H_1$)

*There is a statistically significant difference in mean Von Mises stress between gold-tungsten composites with single inclusion and gold-tungsten composites with multiple inclusions when irradiated at 850 nm wavelength.*

Figures 17, 18 and 19 show the comparison of mean stress values between wavelengths.

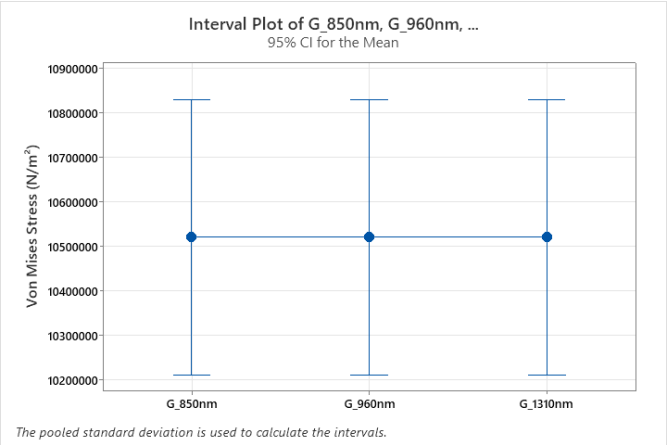


Figure 17. Comparison of gold mean stress value between wavelengths

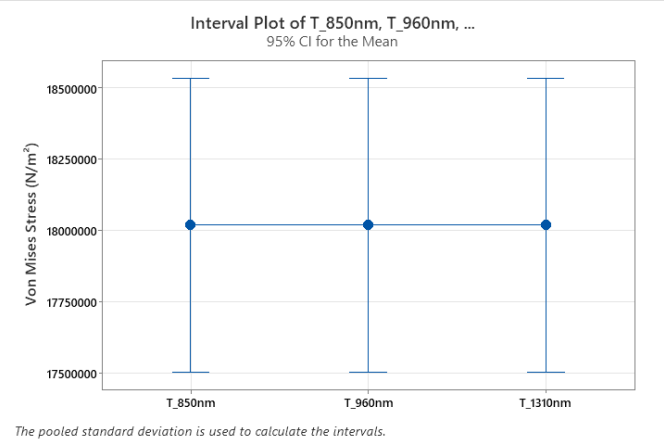


Figure 18. Comparison of gold mean stress value between wavelengths

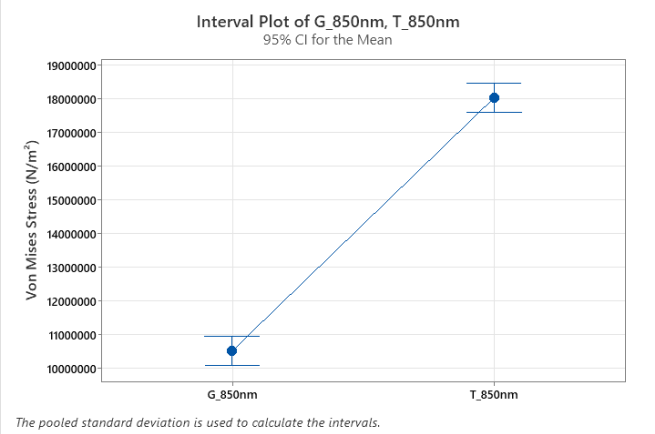


Figure 19. Comparison of mean stress value between material at 850 nm

Figure 20 presents the interval plot comparing the two cases. G_T (S) is the single tungsten inclusion while G_T (M) indicates multiple tungsten inclusions. The plot shows that the means of the two distributions are very close to each other, with the single inclusion case showing a slightly higher mean stress (approximately $1.08 \times 10^8$ N/m²) compared to the multiple inclusions case (approximately $1.06 \times 10^8$ N/m²). The 95% confidence intervals for both cases overlap almost completely, indicating that the stress values for the two configurations fall within similar ranges.

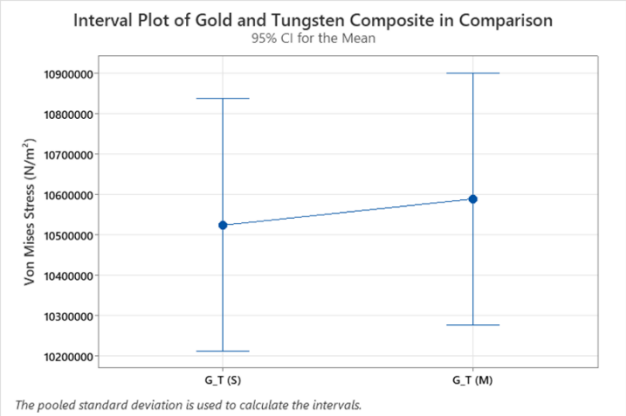


Figure 20. Comparison of mean stress value between the two cases of inclusion

Figure 21 presents the interval plot comparing pure gold, single inclusion composite (G_T(S)), and multiple inclusions composite (G_T(M)). The plot shows that the means of all three distributions are very close to each other, with pure gold exhibiting a mean stress around $1.02 \times 10^8$ N/m², while both composite configurations show slightly higher mean values. The single inclusion case displays a marginally higher mean (approximately $1.08 \times 10^8$ N/m²) compared to the multiple inclusions case (approximately $1.06 \times 10^8$ N/m²). However, the 95% confidence intervals for all three configurations overlap considerably, indicating that the stress values fall within similar ranges. Notably, the interval for the multiple tungsten inclusions is slightly larger than that for the single inclusion, indicating that the presence of multiple inclusions leads to a higher degree of variability in the stress distribution.

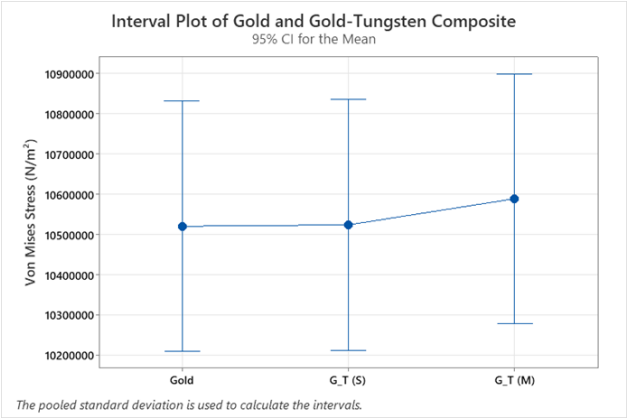


Figure 21. Comparison of mean stress value between pure gold and the two cases of inclusion

### *4. Interpretation of p-values*

Table 5 below is the P-value for each ANOVA test made. The analysis within each material, gold and tungsten, showed no significant differences in stress values across the three tested wavelengths (850 nm, 960 nm, and 1310 nm). The ANOVA test results for both materials gave p-values of 1.000, meaning the small changes in stress are likely due to random variation rather than the effect of wavelength. The 95% confidence intervals also overlapped, and the average stress values were very similar. This outcome is expected, since both gold and tungsten have relatively stable optical absorption across near-infrared (NIR) wavelengths.

On the other hand, a clear difference was found when comparing gold and tungsten at 850 nm. The ANOVA test gave a p-value of 0.000, showing that the stress values between the two materials were significantly different. Tungsten produced much higher stress (around 90 MPa) compared to gold (around 16 MPa). The confidence intervals did not overlap, which supports this difference. Tungsten is much stiffer than gold and absorbs more light at 850 nm. Assume that for 960 nm and 1310nm, the ANOVA test made produced the same results as 850nm.

For the composite models, the ANOVA test comparing single and multiple tungsten inclusions at 850 nm yielded a p-value of 0.773, which is greater than the significance level of 0.05. This indicates no statistically significant difference in mean Von Mises stress between the two configurations. The 95% confidence intervals for both configurations overlapped considerably, further supporting this conclusion.

When comparing pure gold with the gold-tungsten composites (both single and multiple inclusions) at 850 nm, the ANOVA test gave a p-value of 0.943, again exceeding the 0.05 threshold. This demonstrates that there is no significant difference in mean stress between pure gold and the composite materials.

TABLE 5. P-VALUE FOR EACH COMPARISON

| Comparison Type | Material(s) | Wavelength (nm) | P-Value | Conclusion |
|---|---|---|---|---|
| Intra-material Comparison | Gold | 850, 960, 1310 | 1.000 | No significant stress difference across wavelengths |
| Intra-material Comparison | Tungsten | 850, 960, 1310 | 1.000 | No significant stress difference across wavelengths |
| Inter-material Comparison | Gold vs. Tungsten | 850, 960, 1310 | 0.000 | Significant difference in stress between gold and tungsten |
| Intra-composite Comparison | Single Tungsten Inclusion vs. Multiple Tungsten Inclusions | 850 | 0.773 | No significant stress difference between single and multiple inclusions |
| Inter-material Comparison | Pure Gold vs. Gold-Tungsten Composite | 850 | 0.943 | No significant stress difference between pure gold and gold-tungsten composite |

## IV. CONCLUSIONS

The results show that for both gold and tungsten, there is no significant difference in stress across the three tested wavelengths (850 nm, 960 nm, and 1310 nm). This means wavelength has little effect on stress generation within the tested range.

In the comparison between gold and tungsten at 850 nm, tungsten showed much higher stress than gold, confirming that photoacoustic sensing can clearly distinguish between the two materials. Between the wavelengths, 850 nm is the most cost-effective. It is widely available, more affordable and gives reliable results, making it the best choice for practical photoacoustic gold testing.

While the simulation results, dot plots, and interval plots reveal slight visible differences in stress distribution patterns between single and multiple tungsten inclusions, the statistical analysis remains bound to the null hypothesis. With p-values of 0.773 for the inclusion comparison and 0.943 for pure gold versus composites, both exceeding the 0.05 significance level. The statistical evidence ultimately upholds the null hypothesis, demonstrating that photoacoustic sensing can clearly distinguish between pure gold and pure tungsten, but detecting tungsten inclusions within a gold matrix presents a greater challenge, as the composite stress responses fall between those of the pure materials with considerable overlap.

## NOMENCLATURE

| | | |
|---|---|---|
| $I_0$ | Peak laser intensity | $W/m^2$ |
| $\mu_a$ | Absorption coefficient | 1/m |
| $t_p$ | Time at peak of pulse | s |
| $\tau$ | Laser pulse half-duration | s |
| $w$ | Beam radius | m |
| $x_0$, $y_0$ | Laser beam center coordinates | m |

Greek letters

| | | |
|---|---|---|
| $\mu_a$ | Absorption coefficient | 1/m |
| $\tau$ | Laser pulse half-duration | s |

## CONFLICT OF INTEREST

The authors declare that there is no conflict of interest regarding the publication of this paper.

## ACKNOWLEDGEMENT

The authors would like to thank to Universiti Sains Islam Malaysia and ADS research group for their cooperation in this research paper.

## REFERENCES

[1] M. Blakeney, “Chapter 3: Impacts of counterfeiting: commercial, fiscal and socio-economic,” in Counterfeit Goods and Organised Crime, Edward Elgar Publishing, 2023, pp. 30 - 41.

[2] V. Ramachandran, “Counterfeit gold bars discovered in New York City,” NBCUniversal Media, 20 September 2012. [Online]. Available: https://www.nbcnews.com/news/us-news/counterfeit-gold-bars-discovered-new-york-city-flna1b5988405.

[3] S. Mills, “Royal Canadian Mint-stamped gold wafer appears to be fake,” CBC News, 30 10 2017. [Online]. Available: https://www.cbc.ca/news/canada/ottawa/fake-gold-wafer-rbc-canadian-mint-1.4368801.

[4] D. Ren, “How Kingold Jewelry’s fake gold bars slipped through scrutiny in one of China’s biggest loan scams,” South China Morning Post, 7 7 2020. [Online]. Available: https://www.scmp.com/business/companies/article/3092042/explainer-how-kingolds-fake-gold-bars-slipped-through-scrutiny.

[5] I. Bolundut, “GOLD: PROPERTIES, MINERALS, ALLOYS, USES AND RECYCLING,” Revista Minelor – Mining Revue, vol. 28, no. 2, pp. 42-48, 2022. DOI: 10.2478/minrv-2022-0013

[6] G. O. Malaysia, “Pawnbroker Act 1972,” Laws of Malaysia, 1972.

[7] Y. Wang, Y. Zhao and S. Liu, “Compressed Sensing for Biomedical Photoacoustic Imaging:,” Sensors and Devices for Biomedical Image Processing, vol. 24, no. 9, p. 2670, 2024. DOI: https://doi.org/10.3390/s24092670

[8] T. Yang, W. Chen and P. Wang, “A review of all-optical photoacoustic spectroscopy as a gas sensing method,” Applied Spectroscopy Review, vol. 6, no. 2, pp. 147-170, 2021. DOI:https://doi.org/10.1080/05704928.2020.1760875

[9] Y. Huang, R. Zhong, Z. Zhang and L. Huang, “A Novel Electromagnetic Wavelength Measurement Method,” Photonics, vol. 11, no. 9, p. 831, 2024. DOI: https://doi.org/10.3390/photonics11090831

[10] K. L. Muratikov, A. L. Glazov, “Theoretical and experimental investigation of the photoacoustic effect in solids with residual stresses,” Central European Journal of Physics, vol. 1, pp. 485-15, 2003. DOI: 10.2478/BF02475859

[11] M. N. Polyanskiy “Refractiveindex.info database of optical constants,” Scientific Data, vol. 11, no. 94, pp. 1-1, 2024. https://doi.org/10.1038/s41597-023-02898-2